Article

Discovery of allosteric and selective inhibitors of inorganic pyrophosphatase from Mycobacterium tuberculosis

Allan H. Pang, Atefeh Garzan, Martha J. Larsen, Thomas J McQuade, Sylvie Garneau-Tsodikova, and Oleg V Tsodikov

ACS Chem. Biol., **Just Accepted Manuscript** • DOI: 10.1021/acschembio.6b00510 • Publication Date (Web): 13 Sep 2016

Discovery of allosteric and selective inhibitors of inorganic pyrophosphatase from Mycobacterium tuberculosis

Allan H. Pang,[a,†] Atefeh Garzan,[a,†] Martha J. Larsen,[b] Thomas J. McQuade,[b] Sylvie Garneau-Tsodikova,[a,*] and Oleg V. Tsodikov[a,*]

[a] Department of Pharmaceutical Sciences, College of Pharmacy, University of Kentucky, 789 South Limestone Street, Lexington, KY, 40536-0596, USA. [b] Center for Chemical Genomics, High-Throughput Screening Laboratory, Life Sciences Institute, University of Michigan, Ann Arbor, MI, 48109, USA.

[†]These two authors contributed equally to this work.

KEYWORDS Antibacterial discovery, Crystal structure, Drug target, Essential enzyme, Inhibitor binding.

ABSTRACT: Inorganic pyrophosphatase (PPiase) is an essential enzyme that hydrolyzes inorganic pyrophosphate (PP_i), driving numerous metabolic processes. We report a discovery of an allosteric inhibitor (2,4-bis(aziridin-1-yl)-6-(1-phenylpyrrol-2-yl)-*s*-triazine) of bacterial PPiases. Analogues of this lead compound were synthesized to target specifically *Mycobacterium tuberculosis* (*Mtb*) PPiase (*Mt*PPiase). The best analogue (compound **16**) with a K_i of 11 μM for *Mt*PPiase is a species-specific inhibitor. Crystal structures of *Mt*PPiase in complex with the lead compound and one of its analogues (compound **6**) demonstrate that the inhibitors bind in a non-conserved interface between monomers of the hexameric *Mt*PPiase in a yet unprecedented pairwise manner, while the remote conserved active site of the enzyme is occupied by a bound PP_i substrate. Consistent with the structural studies, the kinetic analysis of the most potent inhibitor has indicated that it functions uncompetitively, by binding to the enzyme-substrate complex. The inhibitors appear to allosterically lock the active site in a closed state causing its dysfunctionalization and blocking the hydrolysis. These inhibitors are the first examples of allosteric, species-selective inhibitors of PPiases, serving as a proof-of-principle that PPiases can be selectively targeted.

INTRODUCTION

Inorganic pyrophosphatases (PPiases) are enzymes that are present in all domains of life.[1, 2] They break down pyrophosphate (PP_i) into two molecules of inorganic phosphate (P_i). The hydrolytic action of PPiases drives many key metabolic processes within the cell, where PP_i is a product.[3] These processes include DNA replication and repair, transcription, and fatty acid biosynthesis. The accumulation of PP_i was shown to be detrimental to cells.[4, 5] In bacteria PPiases were demonstrated to be essential enzymes. For example, *E. coli* cells stopped growing when PPiase expression was downregulated by genetic methods.[4, 6, 7] More recently, by high-density transposon mutagenesis, PPiase was shown to be essential for *in vitro* growth of *Mycobacterium tuberculosis* (*Mtb*) both in glycerol and in cholesterol as carbon sources.

PPiases are divided into four structurally distinct families. Families I-III are comprised of cytoplasmic enzymes responsible for PP_i/P_i homeostasis in the cell, and family IV is comprised of integral membrane proton transporting enzymes. Family I PPiases are ubiquitous single-domain enzymes that are hexameric in bacteria and dimeric in eukaryotes. Family II PPiases are two-domain dimeric enzymes present in some bacteria, such as *Staphylococcus aureus*,[8] *Streptococcus sp.*,[9, 10] and *Bacillus subtilis*.[10] The most recently identified family III PPiases are tetramers containing a haloacid dehalogenase domain. These enzymes have been found in only a few representatives of all three domains of life, where these enzymes have likely evolved as a stress response mechanism.[11, 12] Representatives of different families display dramatic differences in their structures and mechanisms. We recently demonstrated that even two bacterial enzymes from the same family, family I, *E. coli* PPiase (*Ec*PPiase) and *Mtb* PPiase (*Mt*PPiase) harbor structural and mechanistic differences in their active sites, in addition to more divergent regions elsewhere in the proteins.[13]

Owing to the above properties, PPiase represents a potential target for developing selective inhibitors as chemical regulators of PP_i/P_i homeostasis or therapeutic agents. However, pursuit of therapeutically or biochemically useful compounds inhibitory to PPiase has not been fruitful yet. Fluoride was identified and extensively studied as an inhibitor of PPiases, with eukaryotic PPiases being more sensitive to fluoride (IC_{50} in the μM range) than bacterial and archaeal PPiases (IC_{50} in the mM range).[14-21] Rigorous structural and functional studies demonstrated that fluoride was bound to the PPiase-PP_i complex at a site proposed to be occupied by a catalytic water molecule, thereby blocking catalysis.[15, 16, 22] Ca^{2+} was also identified as an inhibitor of mammalian and bacterial PPiases.[23, 24] Upon binding PPiase, Ca^{2+} distorts the

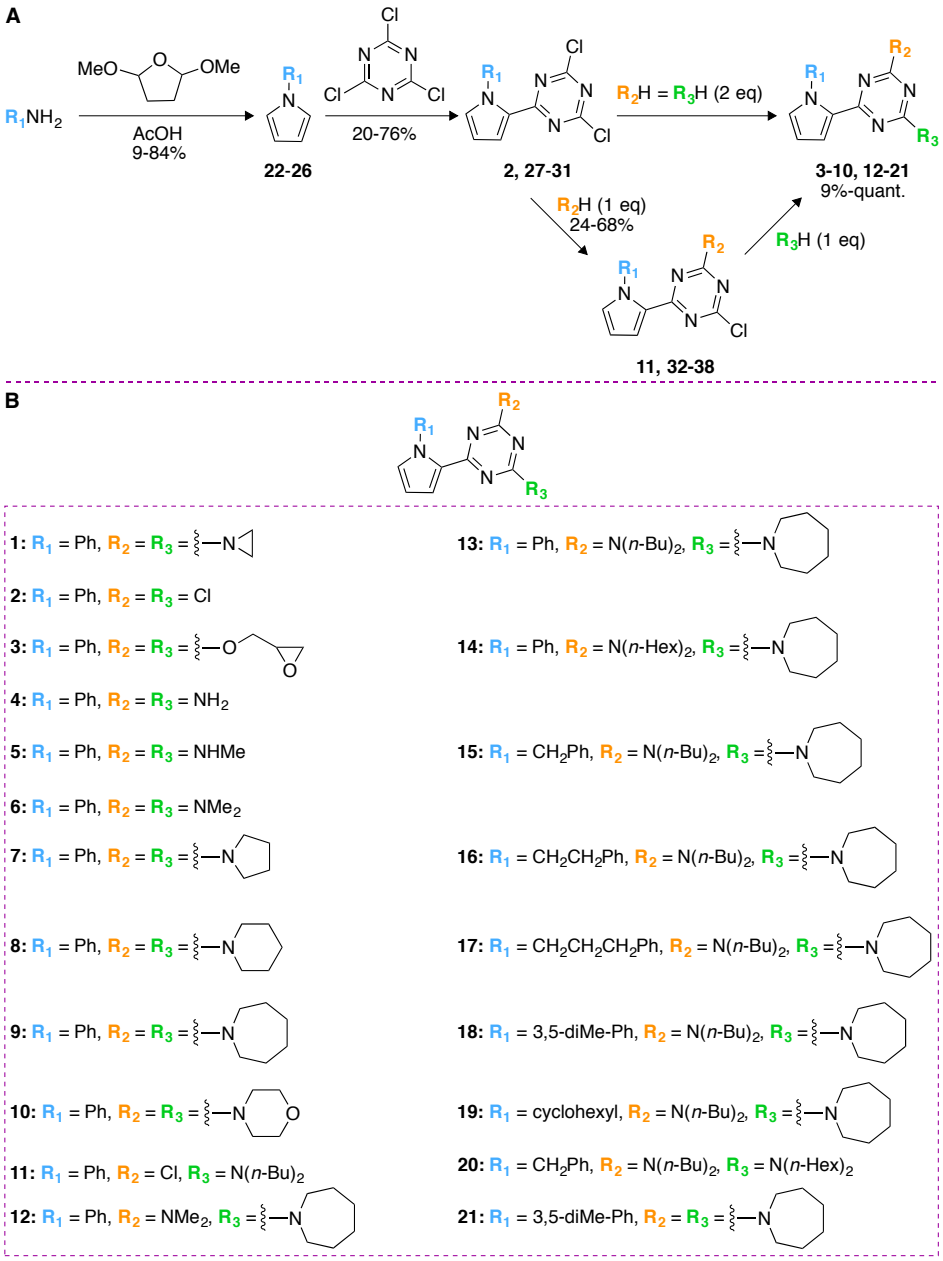

Figure 1. A. The synthetic scheme used to prepare 20 compounds tested for PPiase inhibition. **B.** Structures of the compounds in this study.

conformation of the catalytic site and perturbs the catalytic water, which results in enzyme inactivation.[24] Several phosphoryl group-containing compounds were also shown to inhibit PPiases or function as effectors. ATP, methylenediphosphonate and PP_i were shown to modulate the PP_i hydrolysis, presumably by binding to a basic pocket of *E. coli* PPiase adjacent to its active site. This basic pocket is not conserved in *Mt*PPiase.[25, 26] Methylenediphosphonate and its analogues are potent competitive inhibitors of mammalian PPiase in the μM range.[27] Imidodiphosphate is a competitive inhibitor of PPiases,[28, 29] mimicking PP_i. Methylene diphosphonic acid was shown to inhibit competitively mammalian PPiase.[30] Nucleotidylsulfates are inhibitors of yeast PPiase.[31] Recently, Cushman and co-workers identified the first nonionic compounds that inhibited *Mt*PPiase, which act by an unknown mechanism.[32] However, these compounds lacked selectivity and inhibited bacterial growth by an off-target mechanism. The lack of useful bacterial PPiase inhibitors prompted us to look for novel inhibitory chemical entities.

We recently reported detailed structural and mechanistic characterization of *Mt*PPiase.[13] Differences between prokaryotic and eukaryotic family I PPiases and those among family I enzymes[13] prompted a possibility of discovery of *Mt*PPiase inhibitors that may be species-selective. Here, we report the discovery as well as structural and functional characterization of first allosteric, species-selective inhibitors of *Mt*PPiase.

RESULTS

Identification of a novel inhibitor of *Mt*PPiase

An inhibitor of *Mt*PPiase was identified from the results of an HTS assay for an unrelated enzyme, where *Ec*PPiase was used as a coupled enzyme. The data from this assay were available through an open-source depository MScreen of the Center for Chemical Genomics at the University of Michigan.[33] We tested inhibition of *Mt*PPiase with 14 hit compounds (Fig. S1) and found that only compound **1**, when used at 100 μM, reduced the activity of *Mt*PPiase to a measurable extent. Therefore, we further investigated compound **1** (Fig. 1). This lead compound was tested for

inhibition of family I PPiases: *Mt*PPiase, *Ec*PPiase and *Saccharomyces cerevisiae* PPiase (*Sc*PPiase), and a family II PPiase from *S. aureus* (*Sa*PPiase). Compound **1** was found to inhibit *Mt*PPiase with an IC_{50} of 130 μM (Table 1, Fig. S2). This compound also inhibited *Ec*PPiase, but more weakly (IC_{50} = 233 μM), whereas no inhibition of either *Sc*PPiase or *Sa*PPiase was observed (Fig. S2).

Table 1. The IC_{50} and Hill coefficient *n* of active compounds against *Mt*PPiase, *Ec*PPiase, *Sc*PPiase, and *Sa*PPiase.

	Family I PPiases					Family II PPiase
	*Mt*PPiase		*Ec*PPiase		*Sc*PPiase	*Sa*PPiase
Cpd	IC_{50} (μM)	*n*	IC_{50} (μM)	*n*	IC_{50} (μM)	IC_{50} (μM)
1	130 ± 45	1.0 ± 0.1	233 ± 110	1.0 ± 0.2	355 ± 2	> 600
6 [b]	540 ± 58	1.0 ± 0.1	> 600	N/D [a]	> 600	> 600
9	115 ± 18	1.1 ± 0.2	220 ± 45	1.0 ± 0.1	455 ± 40	> 600
11	110 ± 3	2.4 ± 0.1	357 ± 126	1.0 ± 0.2	> 600	> 600
12	> 600	N/D [a]	431 ± 22	2.1 ± 1.3	> 600	314 ± 7
13	37 ± 5	1.9 ± 0.4	98.2 ± 8	2.2 ± 0.3	300 ± 11	155 ± 23
14	44 ± 5	2.3 ± 0.5	269 ± 8	3.3 ± 0.2	378 ± 12	269 ± 8
15	27 ± 3	1.8 ± 0.3	> 600	N/D [a]	> 600	> 600
16	23 ± 1	1.9 ± 0.2	256 ± 34	1.4 ± 0.2	179 ± 9	109 ± 16
17	36 ± 5	1.7 ± 0.4	221 ± 44	1.1 ± 0.3	293 ± 23	97 ± 16
18	58 ± 4	2.0 ± 0.3	68 ± 8	1.0 ± 0.1	328 ± 34	> 600
19	72 ± 4	1.9 ± 0.2	116 ± 8	3.2 ± 0.6	418 ± 24	360 ± 35
20	> 600	N/D [a]	147 ± 14	1.0 ± 0.1	> 600	> 600
21	166 ± 20	1.0 ± 0.1	492 ± 218	1.0 ± 0.2	> 600	300 ± 17

[a] These values could not be determined due to the lack of detectable inhibition. [b] Compounds **2**-**5**, **7**-**8**, and **10** were not inhibitory to any of the four enzymes.

Crystal structure of *Mt*PPiase in complex with compound 1

The complex of *Mt*PPiase with compound **1** was crystallized in a solution containing molar concentrations of Na^+/K^+ phosphate. The active site did not contain compound **1**; unexpectedly, a strong F_o-F_c electron density corresponding to compound **1** was located in a channel leading to the large central cavity of the *Mt*PPiase hexamer, allowing us to model unambiguously the bound inhibitor **1** (Figs. 2A, 2B, and S3A). This channel is formed by 4 monomers of *Mt*PPiase and contains two bound inhibitors that are related by a crystallographic dyad symmetry. The total of three symmetry-related channels are present in the *Mt*PPiase hexamer, each of which containing a pair of bound inhibitor molecules. The inhibitor molecules are located ~20 Å away from the closest active site (Fig. 2A), which belongs to a monomer that does not contact the inhibitors directly. Furthermore, an inhibitor molecule bound to a given monomer is located on the face opposite to the active site of that monomer, ~24 Å away from the active site. Therefore, these inhibitors must act allosterically.

The two molecules of compound **1** interact with each other by parallel stacking of their coplanar pyrrole and *s*-triazine moieties with the interplanar distance of ~4 Å, with the pyrrole ring of one molecule stacking against the *s*-triazine ring of the other and *vice versa* (Fig. 2B). Furthermore, the inhibitors are in a mostly hydrophobic environment of protein residues. Each inhibitor molecule is sandwiched between protein residues and the other inhibitor molecule. Specifically, the *s*-triazine moiety of one inhibitor molecule is sandwiched by the pyrrole moiety of the other inhibitor on one side and the indole of Trp102 on the other (Fig. 2B). The pyrrole ring of one inhibitor is in contact with the *s*-triazine of the other inhibitor and the carboxyl group of Glu115, otherwise exposed to the central solvent-filled cavity. The phenyl ring is in nonpolar contact with Val105, Pro112, and two aziridine rings, one from the same inhibitor molecule and the other one from the other. Additionally, the phenyl group interacts sterically with the main chain carbonyl oxygen of Asp110. The aziridine ring adjacent to the phenyl group is in a hydrophobic pocket of the aliphatic stem of His104 and Val105 located in a loop region of the closest monomer and Phe114 and Pro112 of the adjacent monomer, which holds the other inhibitor molecule. The main chain carbonyl oxygen of Arg101 interacts electrostatically with the aziridine nitrogen (the O-N distance is 3.6 Å), and it may form a weak hydrogen bond with the protonated form of this amino group. The other aziridine ring is located in the hydrophobic pocket of Pro63, the aliphatic stem of Arg101 and Trp102 of one monomer and Phe114 of the adjacent monomer of *Mt*PPiase. Both aziridine groups are partially solvent-exposed towards the central cavity and the channel exit; therefore, these groups appear to be amenable to larger substitutions.

Strong omit F_o-F_c electron density in the active site of the enzyme unambiguously indicated the presence of a bound PP_i (Fig. S3A), which apparently formed at the high concentrations of P_i in the crystallization solution as a product of the enzymatic reaction in the direction of synthesis. The PP_i substrate is held by a network of electrostatic interactions with Lys16, Arg30, and Lys127, and by direct or water-mediated hydrogen bonds with Tyr42, Glu85, Asp89, and Tyr126 (Fig. 3A). The PP_i is bound similarly to that in our recently reported crystal structure of a *Mt*PPiase-PP_i-Ca^{2+} complex (Fig. 3C; PDB ID: 4Z74[13]).

Optimization of the lead compound

The synthesis of all compounds used in our structure-activity-relationship (SAR) study started by reactions of 2,5-dimethoxytetrahydrofuran with commercially available amines, yielding pyrroles **22**-**26** (Fig. 1). The commercially available 1-phenylpyrrole and our synthesized pyrroles **22**-**26** were reacted with cyanuric chloride to obtain compounds **2** and **27**-**31**, respectively. Compound **2** (R_1 = phenyl) was then reacted with 1 equivalent of amine nucleophiles to generate mono-addition products **11**, **32**, and **33**. Similarly, compounds **27**-**31** afforded molecules **34**-**38**. Compound **2** (R_1 = phenyl) was reacted with 2 equivalents of alcohol and amine nucleophiles to obtain the disubstituted products **3**-**10,** and compound **30** was reacted with 2 equivalents of hexamethyleneimine (also known as azepane) to generate compound **21**. The monosubstituted compounds **32**-**38** were reacted with an additional equivalent of different amines to afford the asymmetric analogues **12** and **14**-**19**. Compounds **11** and **34**

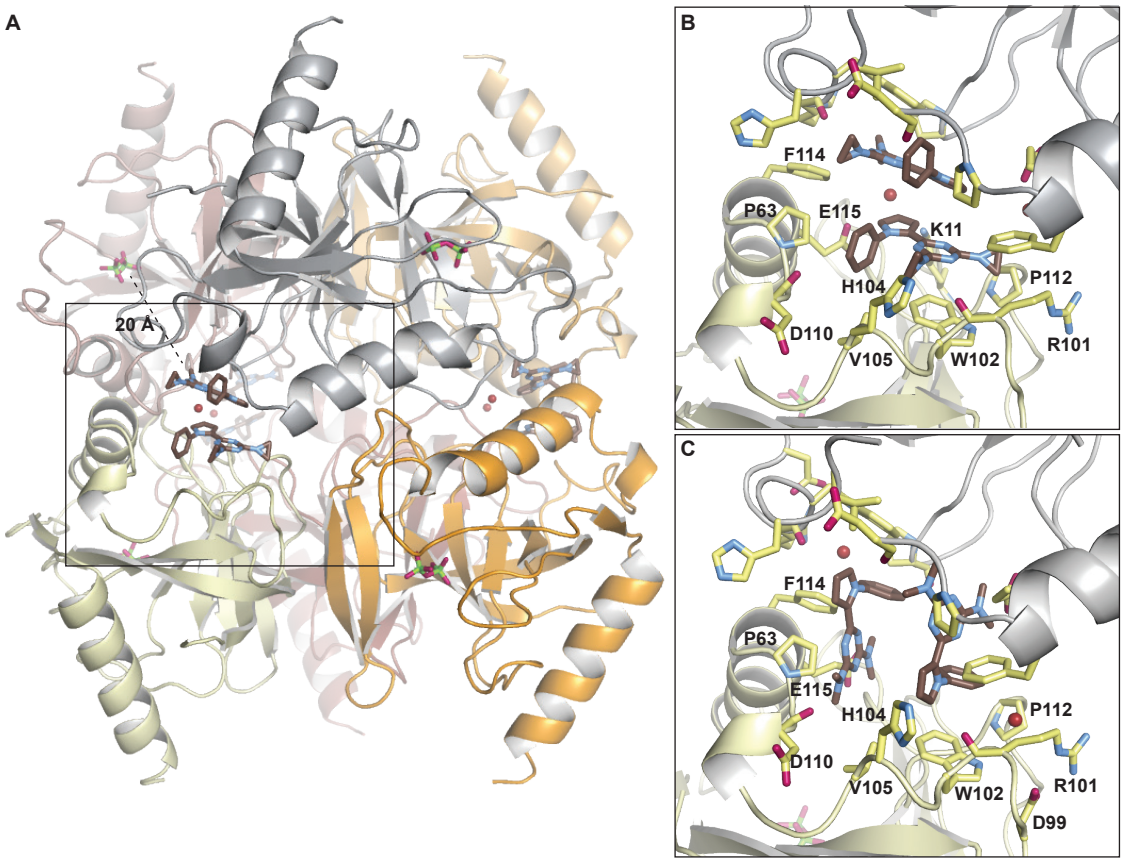

Figure 2. Crystal structures of *Mt*PPiase in complex with compounds **1** and **6**. **A.** The overall view of the *Mt*PPiase hexamer in complex with compound **1**. The inhibitor pair in the black square is located ~20 Å apart from the closest active site. **B.** The inhibitor binding site occupied by compound **1**. **C.** The inhibitor binding site occupied by compound **6**. The inhibitors and the interacting residues of *Mt*PPiase are shown as brown and yellow sticks, respectively. Water molecules are shown as red spheres, PP_i is shown as green sticks in panel A.

were reacted with other amines to yield compounds **13** and **20**, respectively.

These analogues were first tested for inhibition of *Mt*PPiase (Table 1). Compound **1** contains aziridine moieties at positions 2 and 4 of the *s*-triazine ring. Because of partial accessibility of the aziridine moieties to solvent in the structure of the *Mt*PPiase-compound **1** complex, we chose to explore the effect of modifications at these positions. In our initial optimization, we first tested compounds **2** and **3** to probe the essentiality of the nitrogen atom. Compound **3** contains a glycidol moiety, an aziridine mimic. These two compounds did not inhibit *Mt*PPiase. Next, we preserved the nitrogen, by generating analogues with identical substituents at positions 2 and 4: either primary amines (**4**), methylamines (**5**), or dimethylamines (**6**). Neither **4** nor **5** were inhibitory to *Mt*PPiase, while **6** showed weak inhibition, with an IC_{50} of 540 μM. Although **6** was 4 times less potent than our lead compound **1**, this was our first active analogue.

Next, we enlarged the rings at these two positions, by replacing the aziridines of compound **1** with pyrrolidines (**7**), piperidines (**8**), and azepanes (**9**). Inhibition by **7** and **8** was undetectable up to 600 μM. In contrast, compound **9** (IC_{50} = 115 μM) had a potency similar to that of compound **1** (IC_{50} = 130 μM). In an attempt to introduce a hydrogen bonding capacity, we attached a morpholino group (**10**) to the 2 and 4 positions of the *s*-triazine. Compound **10**, however, did not display inhibition of *Mt*PPiase.

Because of the different environments of the two aziridine groups of **1** in the crystal structure of the *Mt*PPiase-compound **1**, complex, we chose to investigate the potency of analogues with asymmetric modifications at positions 2 and 4 of the *s*-triazine. First, we tested compound **11** containing a di-*n*-butylamine and a chlorine. Compound **11** had a comparable IC_{50} (110 μM) to that of compound **9** (IC_{50} = 115 μM). We then kept the azepane group at one position, while modifying the other position. To explore the effect of the size of these substituents, we generated compounds with a dimethylamine (**12**), a di-*n*-butylamine (**13**), and a di-*n*-hexylamine (**14**). Compound **12** with the smallest substituent was not inhibitory. Compounds **13** and **14** had a dramatically increased potency against *Mt*PPiase with IC_{50} values of 37 μM and 44 μM, respectively. Compound **13** with a di-*n*-butylamine and an azepane at positions 2 and 4 of the *s*-triazine was our best *Mt*PPiase inhibitor in that series.

After varying the 2 and 4 positions of the *s*-triazine moiety, we investigated the effect of replacing the phenyl group at position 1 of the pyrrole. We generated analogues with linkers between the pyrrole and the phenyl moiety. The phenyl group was replaced by a benzyl (**15**), a phenethyl (**16**), and a phenylpropyl (**17**) group. Compounds **15** and **16** had improved potency with IC_{50} values of 27 μM and 23 μM, respectively, whereas compound **17** (IC_{50} = 36 μM) was comparably potent to compound **13**. Increasing the size of the substituent, by replacing the azepane of compound **15** by a di-*n*-hexylamine (compound **20**) led to a loss of *Mt*PPiase inhibitory activity. We also replaced the phenyl on the pyrrole by two other substituents, a 3,5-dimethylphenyl (**18**) and a cyclohexyl (**19**). Both compounds remained active (IC_{50} of 58 μM for **18** and 72 μM for **19**), but were inferior to the above compounds.

Three of the best inhibitors, compounds **15**, **16**, and **17**, completely inhibited the enzymatic activity at 100 μM (Fig. 4). Overall, our optimization yielded compound **16** (IC_{50} = 23 μM), which was ~6-fold more potent than our lead compound **1**. Notably, the most potent and some other inhibitors of *Mt*PPiase exhibit dose-

response inhibition with the Hill coefficient (n) of 2 (Table 1), indicating that inhibitors bind pairwise cooperatively. This cooperativity is consistent with the crystal structures that show that inhibitors interact with each other in a pairwise fashion when bound to the enzyme.

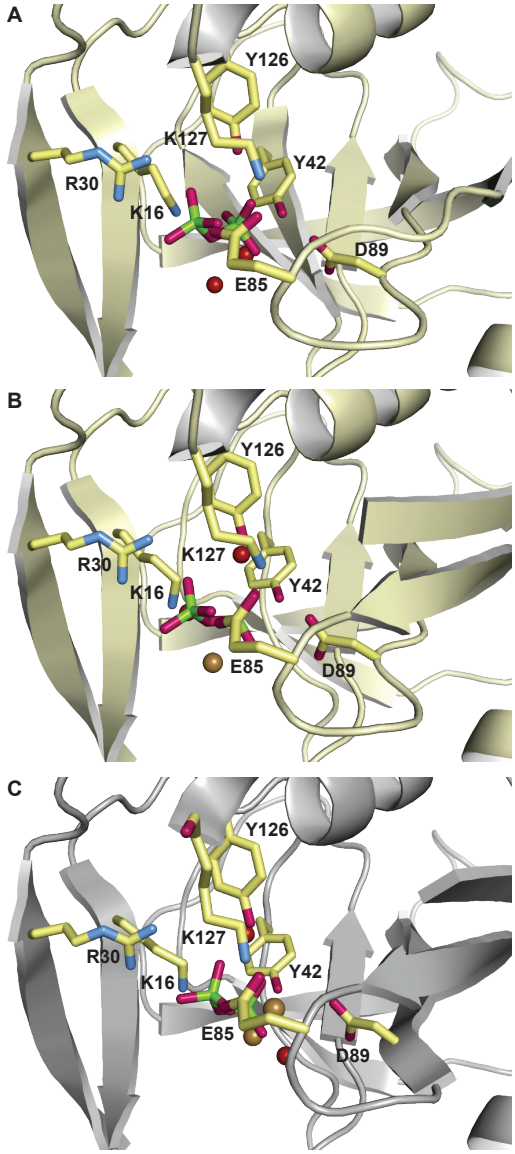

Figure 3. The catalytic site of *Mt*PPiase in different complexes. *Mt*PPiase in complex with **A.** compound **1** and PP_i, **B.** compound **6**, PP_i, and Ca^{2+}, and **C.** PP_i and Ca^{2+} (PDB ID: 4Z74). Ca^{2+} and H_2O are depicted as gold and red spheres, respectively.

Crystal structure of *Mt*PPiase in complex with compound 6

Even though all analogues exhibiting *Mt*PPiase inhibition were tested in co-crystallization or crystal soaking experiments, in addition to compound **1**, only compound **6** bound *Mt*PPiase in the crystalline form. Crystals of a *Mt*PPiase-compound **6** complex were obtained by soaking this compound into crystals of the *Mt*PPiase-$2P_i$-Ca^{2+} complex, obtained as previously reported.[13] To our surprise, we found that a PP_i molecule was identified in the F_o-F_c omit map, instead of two P_i ions (Figs. 3B and S3B). The PP_i is bound similarly to that in the *Mt*PPiase-compound **1** crystal structure. Two bound Ca^{2+} were also found in the active site at locations similar to those of the two Ca^{2+} ions in the *Mt*PPiase-$2P_i$ structure.[13]

Compound **6** was bound in the same site as compound **1** and interacting with its symmetry-related copy, appearing as a dimeric inhibitor. However, the orientation of compound **6** is different to that of compound **1** such that the pyrrole-triazine planes of the two compounds are approximately perpendicular (Fig. 2C). Due to the crystal symmetry, the two molecules of compound **6** in each of the three binding sites are stacked against each other in the same head-to-tail manner as for compound **1**, pyrrole to triazine and *vice versa*. The orientation difference led to an important change in the interactions of the two compounds with the enzyme: compound **6** makes approximately the same number of contacts with each of the two *Mt*PPiase monomers.

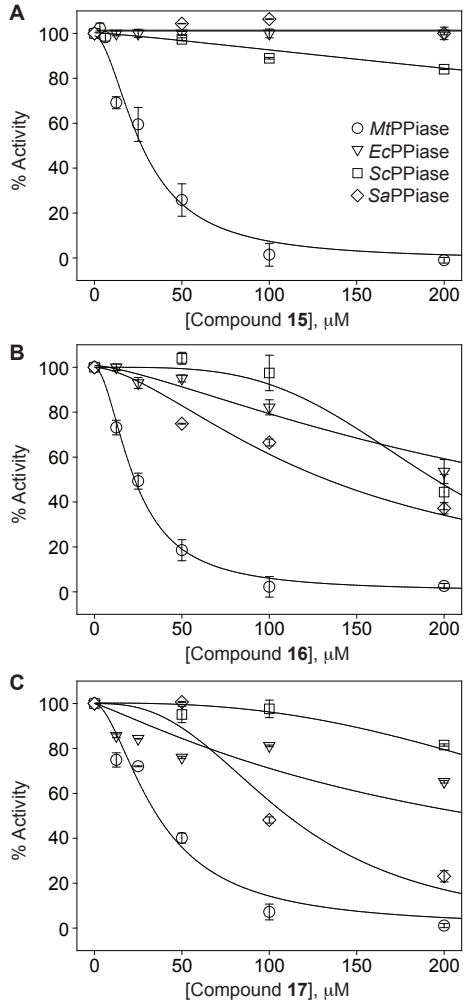

Figure 4. Dose-response assays of inhibition of *Mt*PPiase, *Ec*PPiase, *Sc*PPiase, and *Sa*PPiase by compounds **15** (**A**), **16** (**B**), and **17** (**C**).

The phenyl ring of the compound **6** is parallel to the indole of Trp102, stacking with it. The phenyl group also interacts with Pro63 of the same protein monomer. The pyrrole group stacks orthogonally with Trp102, with Phe114 of another monomer, and makes additional nonpolar contacts with Val105 of the same monomer as for Trp102. The position of the dimethyl amino group that interacts with the phenyl ring is similar to that of the pyrrole group of compound **1**; therefore, the interactions are similar to those described for the pyrrole of compound **1**. The other dimethyl amino group is located near the phenyl group of compound **1**; for this group, one can also refer to the interactions with the protein that have already been described for compound **1**.

Mode of Inhibition

We investigated the mechanism of inhibition by the most potent compound (**16**) by a series of steady-state kinetic experiments at different inhibitor and substrate (PP_i) concentrations (Fig. 5A). At each inhibitor concentration, the rate of hydrolysis as a function of

PP_i concentration obeyed Michaelis-Menten kinetics (Fig. 5A). The simultaneous analysis of the kinetic data for all inhibitor and substrate concentrations is most consistent with the uncompetitive mode of inhibition, where the inhibitor binds the binary *Mt*PPiase-PP_i complex, preventing the hydrolytic step. An analogous analysis of the data assuming noncompetitive inhibition yielded inadequate fit to the data for the highest inhibitor concentration (Fig. S4). The uncompetitive inhibition is signified by characteristic parallel linear kinetics for different inhibitor concentrations in double reciprocal (Lineweaver-Burk) coordinates ($1/V$ *vs* $1/[S]$) (Fig. 5B). The global analysis of all the data yielded the best-fit value of the equilibrium constant for binding of compound **16** to the *Mt*PPiase-PP_i complex $K_i = 11.4 \pm 1.6$ μM. The uncompetitive inhibition mode is in excellent agreement with the structural observations of PP_i bound in the active site of the *Mt*PPiase-inhibitor complexes.

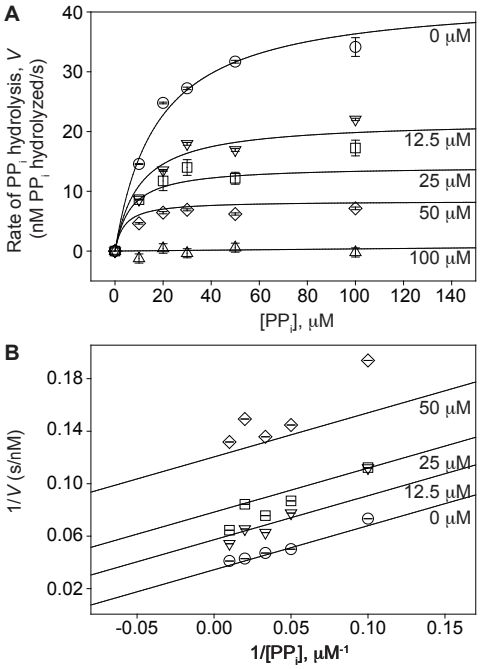

Figure 5. Mode of inhibition studies with compound **16**. **A.** Steady-state measurements of reaction rate at different concentrations of compound **16,** as specified. **B.** The Lineweaver-Burk plot (1/V vs 1/[S]) of the data in panel A. The best-fit curves correspond to: $k_{cat} = 44 \pm 4$ s^{-1} (in P_i formed), $K_m = 18 \pm 4$ μM, and $K_i = 11.4 \pm 1.6$ μM.

The species selectivity of the allosteric PPiase inhibitors

To test whether the allosteric *Mt*PPiase inhibitors can inhibit PPiases from other organisms, we performed dose-response assays with all 20 analogues and another family I prokaryotic PPiase (*Ec*PPiase), family I eukaryotic PPiase (*Sc*PPiase), and family II PPiase (*Sa*PPiase) (Table 1, Figs. 4 and S2).

The binding site for these compounds is not conserved in the eukaryotic *Sc*PPiase and the family II *Sa*PPiase, which form oligomers of a different type (Fig. S5). As expected, these compounds are poor inhibitors of these enzymes, displaying modest to high selectivity for *Mt*PPiase over *Sc*PPiase or *Sa*PPiase. The best analogue that inhibits *Sc*PPiase is compound **16** with an IC_{50} of 179 μM, ~8-fold less potent against this enzyme than against *Mt*PPiase (Table 1, Fig. 4B). For *Sa*PPiase, the most potent inhibition was displayed by compound **17** with an IC_{50} of 97 μM, making it ~3-fold less potent than against *Mt*PPiase (Fig. 4C). Compound **15**, which is one of the most potent *Mt*PPiase inhibitors, is also one of the most selective ones, exhibiting >20-fold higher potency against *Mt*PPiase than against either *Sc*PPiase or *Sa*PPiase (Fig. 4A).

*Ec*PPiase is a family I PPiase with a similar hexameric organization to that of *Mt*PPiase, but moderate conservation of the structurally analogous *Ec*PPiase residues to those that interact with the inhibitors *Mt*PPiase (Fig. S6A,B). Generally, the tested compounds displayed modest to high selectivity for *Mt*PPiase over *Ec*PPiase, but there were a few exceptions. Compounds **19** and **20** were modestly potent against *Ec*PPiase, but highly selective for it over *Mt*PPiase. Compound **18**, which was the most potent inhibitor of *Ec*PPiase, was ~2-3-fold more potent than the above compounds, but it inhibited *Ec*PPiase and *Mt*PPiase similarly. Compounds **15** and **16** that were most potent against *Mt*PPiase were highly selective against this enzyme over *Ec*PPiase, >20-fold and 10-fold, respectively.

DISCUSSION

Discovery of allosteric PPiase inhibitors

PPiase is an enzyme that is essential in most bacteria and, therefore, it represents an attractive potential target for inhibition. However, the active site of the enzyme is highly charged and relatively small, evolved to accept a charged PP_i substrate with high selectivity over larger pyrophosphate group containing metabolites. The lack of a small hydrophobic cavity that could bind drug-like molecules competitively with PP_i has likely impeded discovery of useful inhibitory compounds. In addition, conservation of the active site in bacterial and eukaryotic PPiases raises a concern about potential off-target effects of inhibition of the human PPiase by bacterial PPiase inhibitors targeting the active site. By mining HTS assay data where PPiases were used as coupled enzymes, we identified novel inhibitors of *Mt*PPiase, with an *s*-triazine core. Remarkably, these inhibitors bind the enzyme cooperatively and interact with each other in a pairwise fashion when bound at symmetrical sites in the subunit interfaces of *Mt*PPiase, which are distant from the active site. This binding mode would have been impossible to obtain by *in silico* screening methods, which dock individual molecules. The SAR study demonstrated that the hydrophobic substituents were necessary for maximum potency among the compounds tested, consistent with the structural observations of predominantly nonpolar contacts between the inhibitors and the enzyme. A box-like shape formed by the two juxtaposed inhibitor cores fits well the intersubunit channel of *Mt*PPiase. This general shape is preserved in the two orthogonal binding modes seen in the crystal structures of *Mt*PPiase-compound **1** and *Mt*PPiase-compound **6** complexes. The two different orientations underscore the major role of hydrophobic surface complementarity in the inhibitor binding.

The structural basis for the allosteric inhibition

Crystals of a *Mt*PPiase-compound **6**-PP_i complex were formed by soaking the inhibitor into crystals of *Mt*PPiase-$2P_i$ complex.[13] Upon inhibitor-enzyme co-crystallization with compound **1** or compound **6** soaking, PP_i formed by the reaction reverse to the hydrolysis stably bound to the enzyme, apparently with a higher affinity than P_i. The significant reversibility of the PP_i hydrolysis catalyzed by bacterial PPiase was demonstrated previously by direct measurements of the quantities of the reaction species.[34] The presence of bound PP_i in the structures of *Mt*PPiase-inhibitor complexes is in excellent agreement with the kinetic data, which indicate that the most potent inhibitor acts uncompetitively, *i.e.*, by binding to the enzyme-substrate complex. Binding of the inhibitor in the intersubunit interface must allosterically hinder the hydrolysis of the substrate by overstabilizing it in the active site and/or by structurally disorganizing the catalytic residues of the enzyme in the substrate bound state. How does the inhibitor binding affect the active site located 20 Å away? In order to answer this question, we compared the structures of the *Mt*PPiase-inhibitor-PP_i complexes with our recently reported structures of a *Mt*PPiase-PP_i complex.[13] The superimposition of the structures of

*Mt*PPiase-compound **6**-PP_i and *Mt*PPiase-PP_i indicated that two active site loops (residues 52-59 and 83-90) that bear catalytically important residues are shifted closer to each other in the complex with the inhibitor, closing slightly the active site (Fig. 6). These conformations of the two loops resemble those in our recently reported structure of *Mt*PPiase-$2P_i$ complex.[13] As in that study, this conformational difference cannot be an artifact of crystal packing interactions,[13] nor an effect of Ca^{2+}, since Ca^{2+} at was present in the reported *Mt*PPiase-PP_i crystals as well as in this *Mt*PPiase-compound **6**-PP_i crystals. Furthermore, in the crystals of the complex with compound **1**, which was formed in the absence of Ca^{2+}, the conformations of these two loops are the same as in the complex with compound **6**. The bound PP_i in the structure of the enzyme-inhibitor complex is shifted in concert with the loop shift towards the positively charged wall with respect to the PP_i in the *Mt*PPiase-PP_i structure. The shift in this direction of the two P_i ions was also seen in the *Mt*PPiase-$2P_i$ structure, which mimicked the enzyme-product complex. These conformational changes are apparently inconsistent with the hydrolytic function of the enzyme, while still favoring substrate binding. The conformational changes of the protein backbone at the inhibitor binding site are much smaller. The side chains of His104, Phe114, and Glu115 are in a different conformation from those in the reported structures of *Mt*PPiase without inhibitors (Fig. S6C), to allow inhibitor access to the otherwise blocked intersubunit channel.[13] We propose that these conformational changes upon inhibitor binding cause subtle changes in angles of secondary structural elements, which propagate to the active site to trigger significant (~2 Å) movements of active site loops and block the hydrolytic step.

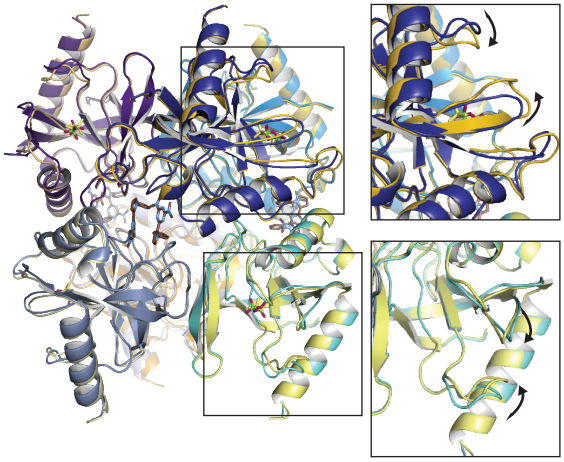

Figure 6. Superimposition of the structures of *Mt*PPiase-compound **6**-PP_i (protein in yellow, PP_i as green sticks) and *Mt*PPiase-PP_i (protein in blue, PP_i as yellow sticks) complexes. The conformational differences in the two active site loops are indicated by the curved arrows.

Proof of principle of PPiase inhibition selectivity

It has been established that the oligomeric organization of bacterial family I PPiase differs from that of PPiases from other families or that of eukaryotic family I PPiases (Fig. S5). Specifically, the inhibitor binding site is present only in family I PPiases. The inhibitory compounds described here are a proof-of-principle that one can selectively target only certain bacterial PPiases while sparing eukaryotic counterparts. The inhibitor binding site contains several residues that are different between *Mt* and *Ec*PPiase (Fig. S6B). Because this site is only partially conserved, the selectivities of different inhibitors against the two enzymes vary (Table 1), and one can expect that both narrow- and broad-spectrum antibacterials may emerge from inhibitory agents targeting this allosteric site.

CONCLUSION

Ubiquitous family I PPiases are critical enzymes for bacterial growth and, therefore, are attractive potential targets. However, a highly charged active site could not be easily targeted by drug-like small molecules. We identified a non-conserved inhibitor binding site in *Mt*PPiase located in the intersubunit interface distant from the active site. The lack of conservation of this allosteric site explains the selectivity of some of the inhibitors even for different family I PPiases. A combination of kinetic and structural studies revealed the uncompetitive mode of inhibition and suggested the molecular mechanism of the allostery. Future studies will evaluate antibacterial activity of the PPiase inhibitors and validate the mechanism of cell growth inhibition as well as test compound toxicity and selectivity. In conclusion, this discovery opens new avenues for development of broad- and narrow-spectrum inhibitors of bacterial PPiases into antibacterial agents, selective metabolic regulators, and chemical probes.

ASSOCIATED CONTENT

Supporting Information. Experimental procedures for (i) the synthesis and characterization of all compounds tested and their intermediates, (ii) cloning, overexpression, and purification of *Ec*PPiase, (iii) preparation of *Mt*PPiase, *Sa*PPiase, and *Sc*PPiase, (iv) inhibition studies, (v) crystallization of *Mt*PPiase in complex with compounds **1** and **6**, and (vi) diffraction data collection and processing. Figures showing the structures of the 14 initial compounds tested for PPiase inhibition (Fig. S1), dose-response assay data (Fig. S2), electron density maps for bound inhibitors **1** and **6** and PP_i (Fig. S3), fit to noncompetitive inhibition (fig. S4), oligomeric organization of different PPiases (Fig. S5), structure of inhibitor binding site (Fig. S6), and 1H and 13C NMR of all molecules synthesized and tested (Figs. S7-S46) are provided. A table of crystallographic information (Table S1) is also presented. Coordinates and structure factor amplitudes for the *Mt*PPiase-compound **1**-PP_i and *Mt*PPiase-compound **6**-PP_i complexes have been deposited in the Protein Data Bank under accession codes 5KDE and 5KDF, respectively. This material is available free of charge via the Internet at http://pubs.acs.org.

AUTHOR INFORMATION

Corresponding Author

sylviegtsodikova@uky.edu
oleg.tsodikov@uky.edu

Funding Sources

This project was supported by startup funds from the College of Pharmacy at the University of Kentucky (to S.G.-T. and O.V.T).

Notes

The authors declare no competing financial interest.

ACKNOWLEDGMENT

This project was supported by startup funds from the College of Pharmacy at the University of Kentucky (to S.G.-T. and O.V.T).

ABBREVIATIONS

Ec, *Escherichia coli*; HTS, high-throughput screening; *Mt* or *Mtb*, *Mycobacterium tuberculosis*; P_i, inorganic phosphatase; PP_i, inorganic pyrophosphatase; PPiase, inorganic pyrophosphatase; *Sa*, *Staphylococcus aureus*; SAR, structure-activity-relationship; *Sc*, *Saccharomyces cerevisiae*.

REFERENCES

1. Cooperman, B. S. (1982) The mechanism of action of yeast inorganic pyrophosphatase, *Methods Enzymol. 87*, 526-548.

2. Lahti, R. (1983) Microbial inorganic pyrophosphatases, *Microbiol. Rev. 47*, 169-178.
3. Kornberg A. On the metabolic significance of phosphorolytic and pyrophosphorolytic reactions. In: Kasha H, Pullman B (eds) Horizons in biochemistry. Academic Press, New York, 1962; pp 251-264.
4. Chen, J., Brevet, A., Fromant, M., Leveque, F., Schmitter, J. M., Blanquet, S., and Plateau, P. (1990) Pyrophosphatase is essential for growth of *Escherichia coli*, *J. Bacteriol. 172*, 5686-5689.
5. Lundin, M., Baltscheffsky, H., and Ronne, H. (1991) Yeast PPA2 gene encodes a mitochondrial inorganic pyrophosphatase that is essential for mitochondrial function, *J. Biol. Chem. 266*, 12168-12172.
6. Sassetti, C. M., Boyd, D. H., and Rubin, E. J. (2003) Genes required for mycobacterial growth defined by high density mutagenesis, *Mol. Microbiol. 48*, 77-84.
7. Griffin, J. E., Gawronski, J. D., Dejesus, M. A., Ioerger, T. R., Akerley, B. J., and Sassetti, C. M. (2011) High-resolution phenotypic profiling defines genes essential for mycobacterial growth and cholesterol catabolism, *PLoS Pathog. 7*, e1002251.
8. Gajadeera, C. S., Zhang, X., Wei, Y., and Tsodikov, O. V. (2015) Structure of inorganic pyrophosphatase from *Staphylococcus aureus* reveals conformational flexibility of the active site, *J. Struct. Biol. 189*, 81-86.
9. Rantanen, M. K., Lehtio, L., Rajagopal, L., Rubens, C. E., and Goldman, A. (2007) Structure of the *Streptococcus agalactiae* family II inorganic pyrophosphatase at 2.80 Å resolution, *Acta Crystallogr. D 63*, 738-743.
10. Fabrichniy, I. P., Lehtio, L., Salminen, A., Zyryanov, A. B., Baykov, A. A., Lahti, R., and Goldman, A. (2004) Structural studies of metal ions in family II pyrophosphatases: the requirement for a Janus ion, *Biochemistry 43*, 14403-14411.
11. Lee, H. S., Cho, Y., Kim, Y. J., Lho, T. O., Cha, S. S., Lee, J. H., and Kang, S. G. (2009) A novel inorganic pyrophosphatase in *Thermococcus onnurineus* NA1, *FEMS Microbiol. Lett. 300*, 68-74.
12. Huang, H., Patskovsky, Y., Toro, R., Farelli, J. D., Pandya, C., Almo, S. C., Allen, K. N., and Dunaway-Mariano, D. (2011) Divergence of structure and function in the haloacid dehalogenase enzyme superfamily: Bacteroides thetaiotaomicron BT2127 is an inorganic pyrophosphatase, *Biochemistry 50*, 8937-8949.
13. Pratt, A. C., Dewage, S. W., Pang, A. H., Biswas, T., Barnard-Britson, S., Cisneros, G. A., and Tsodikov, O. V. (2015) Structural and computational dissection of the catalytic mechanism of the inorganic pyrophosphatase from *Mycobacterium tuberculosis*, *J. Struct. Biol. 192*, 76-87.
14. Hachimori, A., Fujii, T., Ohki, K., and Iizuka, E. (1983) Purification and properties of inorganic pyrophosphatase from porcine brain, *J. Biochem. 93*, 257-264.
15. Baykov, A. A., Artjukov, A. A., and Avaeva, S. M. (1976) Fluoride inhibition of inorganic pyrophosphatase. I. Kinetic studies in a Mg^{2+}-PP_i system using a new continuous enzyme assay, *Biochim. Biophys. Acta 429*, 982-992.
16. Baykov, A. A., Bakuleva, N. P., Nazarova, T. I., and Avaeva, S. M. (1977) Fluoride inhibition of inorganic pyrophosphatase. II. Isolation and characterization of a covalent intermediate between enzyme and entire substrate molecule, *Biochim. Biophys. Acta 481*, 184-194.
17. Oliva, G., Romero, I., Ayala, G., Barrios-Jacobo, I., and Celis, H. (2000) Characterization of the inorganic pyrophosphatase from the pathogenic bacterium *Helicobacter pylori*, *Arch. Microbiol. 174*, 104-110.
18. Schwarm, H. M., Vigenschow, H., and Knobloch, K. (1986) Purification and properties of a soluble inorganic pyrophosphatase from *Rhodopseudomonas palustris*, *Biol. Chem. 367*, 119-126.
19. van Alebeek, G. J., Keltjens, J. T., and van der Drift, C. (1994) Purification and characterization of inorganic pyrophosphatase from *Methanobacterium thermoautotrophicum* (strain delta H), *Biochim. Biophys. Acta 1206*, 231-239.
20. Josse, J. (1966) Constitutive inorganic pyrophosphatase of *Escherichia coli*. 1. Purification and catalytic properties, *J. Biol. Chem. 241*, 1938-1947.
21. Tominaga, N., and Mori, T. (1977) Purificantion and characterization of inorganic pyrophosphatase from *Thiobacillus thiooxidans*, *J. Biochem. 81*, 477-483.
22. Samygina, V. R., Moiseev, V. M., Rodina, E. V., Vorobyeva, N. N., Popov, A. N., Kurilova, S. A., Nazarova, T. I., Avaeva, S. M., and Bartunik, H. D. (2007) Reversible inhibition of *Escherichia coli* inorganic pyrophosphatase by fluoride: trapped catalytic intermediates in cryo-crystallographic studies, *J. Mol. Biol. 366*, 1305-1317.
23. Baykov, A. A., Volk, S. E., and Unguryte, A. (1989) Inhibition of inorganic pyrophosphatase of animal mitochondria by calcium, *Arch. Biochem. Biophys. 273*, 287-291.
24. Avaeva, S. M., Vorobyeva, N. N., Kurilova, S. A., Nazarova, T. I., Polyakov, K. M., Rodina, E. V., and Samygina, V. R. (2000) Mechanism of Ca^{2+}-induced inhibition of Escherichia coli inorganic pyrophosphatase, *Biochemistry 65*, 373-387.
25. Rodina, E. V., Vorobyeva, N. N., Kurilova, S. A., Sitnik, T. S., and Nazarova, T. I. (2007) ATP as effector of inorganic pyrophosphatase of *Escherichia coli*. The role of residue Lys112 in binding effectors, *Biochemistry. 72*, 100-108.
26. Rodina, E. V., Vorobyeva, N. N., Kurilova, S. A., Belenikin, M. S., Fedorova, N. V., and Nazarova, T. I. (2007) ATP as effector of inorganic pyrophosphatase of *Escherichia coli*. Identification of the binding site for ATP, *Biochemistry. 72*, 93-99.
27. Smirnova, I. N., Kudryavtseva, N. A., Komissarenko, S. V., Tarusova, N. B., and Baykov, A. A. (1988) Diphosphonates are potent inhibitors of mammalian inorganic pyrophosphatase, *Arch. Biochem. Biophys. 267*, 280-284.
28. Zyryanov, A. B., Lahti, R., and Baykov, A. A. (2005) Inhibition of family II pyrophosphatases by analogs of pyrophosphate and phosphate, *Biochemistry 70*, 908-912.
29. Kelly, S. J., Feldman, F., Sperow, J. W., and Butler, L. G. (1973) Kinetic effects of inorganic pyrophosphate analogs on several inorganic pyrophosphate hydrolyzing enzymes, *Biochemistry 12*, 3338-3341.
30. Komissarenko, S. V., Gulaia, N. M., and Gubenko, E. P. (1977) Inhibition of mouse spleen inorganic pyrophosphatase by methylene diphosphonic acid, *Biokhimiia 42*, 238-242.
31. Shoyab, M., and Marx, W. (1971) Inhibition of yeast inorganic pyrophosphatase by nucleotidylsulfates, *Arch. Biochem. Biophys. 146*, 71-75.
32. Lv, W., Banerjee, B., Molland, K. L., Seleem, M. N., Ghafoor, A., Hamed, M. I., Wan, B., Franzblau, S. G., Mesecar, A. D., and Cushman, M. (2014) Synthesis of 3-(3-aryl-pyrrolidin-1-yl)-5-aryl-1,2,4-triazines that have antibacterial activity and also inhibit inorganic pyrophosphatase, *Bioorg. Med. Chem. 22*, 406-418.
33. Jacob, R. T., Larsen, M. J., Larsen, S. D., Kirchhoff, P. D., Sherman, D. H., and Neubig, R. R. (2012) MScreen: an integrated compound management and high-throughput screening data storage and analysis system, *J. Biomol. Screen. 17*, 1080-1087.
34. Baykov, A. A., Shestakov, A. S., Kasho, V. N., Vener, A. V., and Ivanov, A. H. (1990) Kinetics and thermodynamics of

catalysis by the inorganic pyrophosphatase of *Escherichia coli* in both directions, *Eur. J. Biochem. 194*, 879-887.

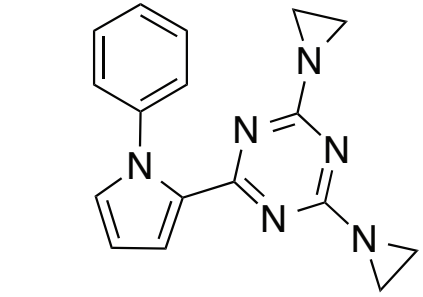

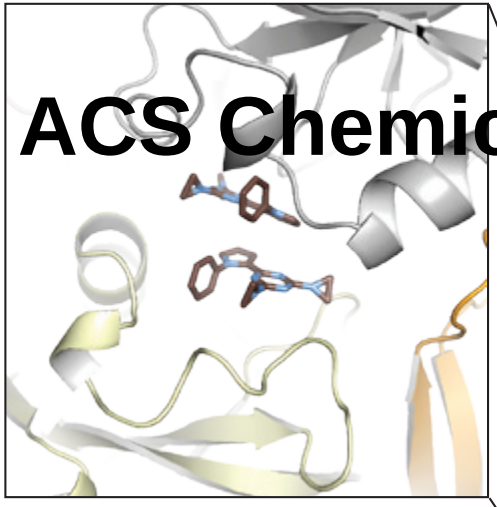

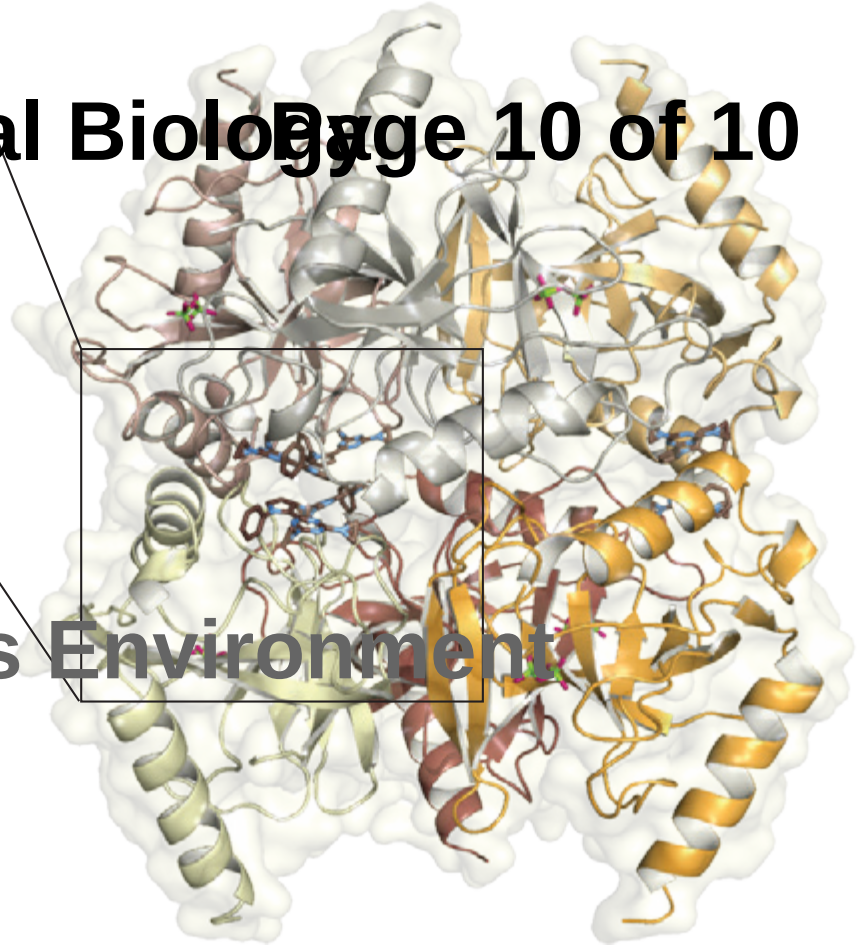

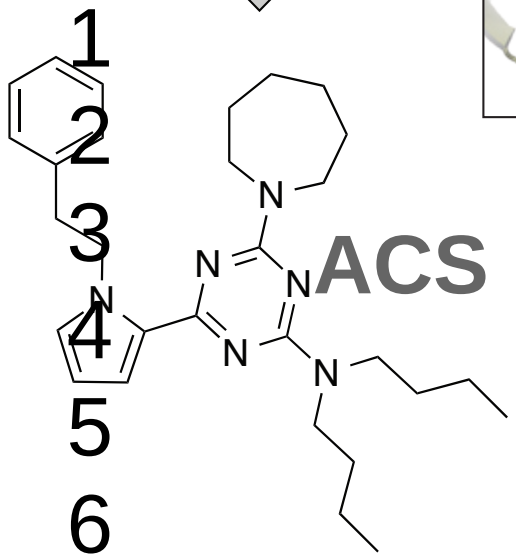

ACS Paragon Plus Environment